Nano Research
2023, 16(3): 3719–3729

ISSN 1998-0124 CN 11-5974/O4
https://doi.org/10.1007/s12274-022-4923-0

Research Article

Catalytic reductive amination of furfural to furfurylamine on robust ultra-small Ni nanoparticles

Yinze Yang[1,2,3], Leilei Zhou[1,2,3], Xinchao Wang[1,2,3], Liyan Zhang[1,2,3], Haiyang Cheng[1,3] (✉), and Fengyu Zhao[1,2,3] (✉)

[1] *State Key Laboratory of Electroanalytical Chemistry, Changchun Institute of Applied Chemistry, Chinese Academy of Sciences, Changchun 130022, China*
[2] *School of Applied Chemistry and Engineering, University of Science and Technology of China, Hefei 230026, China*
[3] *Jilin Province Key Laboratory of Green Chemistry and Process, Changchun Institute of Applied Chemistry, Chinese Academy of Sciences, Changchun 130022, China*

Received: 8 July 2022 / **Revised:** 9 August 2022 / **Accepted:** 16 August 2022

ABSTRACT

The synthesis of primary amines via reductive amination in the presence of NH_3 and H_2, as a green and sustainable process, has attracted much attention. In this paper, we prepared series of Ni/SiO_2 catalysts with deposition-precipitation and impregnation methods, and their catalytic performances on the reductive amination of a biomass derived compound of furfural to produce furfurylamine were studied. The catalytic activity and the yield were correlated to the structure and the surface properties of catalysts largely. The Ni/SiO_2 is of high Lewis acidity and small Ni particle with numerous large Ni flat step surface showed high activity and selectivity, it afforded a reaction rate of 12.8 h^{-1} and a high yield to furfurylamine around 98%. These results are superior to the most non-noble metal catalysts reported so far. Moreover, the reaction route was examined with the unit control reactions of the intermediate. To produce furfurylamine selectively, the most suitable catalyst should have the moderate but not the highest activity in activation of hydrogen and hydrogenation in the reductive amination of furfural. This work provides some useful information for the catalytic reductive amination of aldehydes both in the design of catalyst and the reaction route.

KEYWORDS

Ni nanoparticle, reductive amination, furfural, furfurylamine

1 Introduction

Primary amines are important chemicals and widely applied as building blocks in synthesis of dyes, agrochemicals, drugs, detergent, and polymers [1, 2]. For the synthesis of primary amines, there are several synthetic methods such as reductive amination of carbonyl compounds [3–9] and alcohols [10–13], hydroamination of olefins [14], amination of aryl halides [15], and reduction of specific nitrogen sources (e.g., oxime [16], amides [17], nitriles [18], and nitro compounds [19–24]). Among these methods, the reductive amination of carbonyl compounds with ammonia (NH_3) as the nitrogen resource and H_2 as reductant is the most attractive and practical route both in industry and academic laboratories. The reductive amination method is of such merits as (1) carbonyl compounds, NH_3, and H_2 are all inexpensive and widely available raw materials; (2) it can proceed at relatively mild conditions (relatively lower temperature and pressure). However, this method generally suffers from a main problem that the chemoselectivity is difficult to control as the initially-generated primary amines are more nucleophilic than NH_3, thus secondary and tertiary amines are easily produced, besides, trimers and alcohols as byproducts are also produced during reaction (Scheme 1) [3, 25, 26]. Therefore, it reminds a big challenge in the development of highly active and selective heterogeneous catalysts to produce primary amines selectively. More recently, various catalysts were developed for the reductive amination of carbonyl compounds, and some progresses have been achieved. Generally, when the catalyst has strong hydrogenation activity, such as Pd and Pt, the secondary amines and/or alcohols could be mainly produced instead of the primary amines [6, 8, 27–29]. On the contrary, when the catalyst has low hydrogenation activity, the intermediates of the primary imine are difficult to hydrogenate to primary amines but trimerize to form trimers [26]. Ru catalysts with moderate hydrogenation activity are usually used to catalyze carbonyl compounds to primary amines. The oxidation state/acidity or electron density of Ru is the main factor in controlling the formation of primary amines. For example, Xu et al. reported that the interfacial electronic effects between Ru and the edge surface of boron nitride lead to a high yield to furfuryl amine (FAM) (90.2%) over the Ru/BN-e catalyst [30]. Hara et al. proposed that the low electron density of Ru (positive charges) on Nb_2O_5 surface may affect the adsorption of furan rings and/or activity of the adsorbed hydrogen atoms for the selective reductive amination of furfural (FAL) over Ru/Nb_2O_5, and gave high yield of FAM (99%) [26]. Thereafter, they demonstrated that the surface acid sites but not the dispersion or oxidation/electronic states of Ru played important role in controlling the formation of FAM over $Ru/Nb_2O_5{\cdot}nH_2O$ catalyst. For $Ru/Nb_2O_5{\cdot}nH_2O$, with increasing reduction temperature from 300 to 400 °C, there was no significant difference in Ru dispersion or oxidation and electronic states, but the amount of acid sites on

Address correspondence to Haiyang Cheng, hycyl@ciac.ac.cn; Fengyu Zhao, zhaofy@ciac.ac.cn

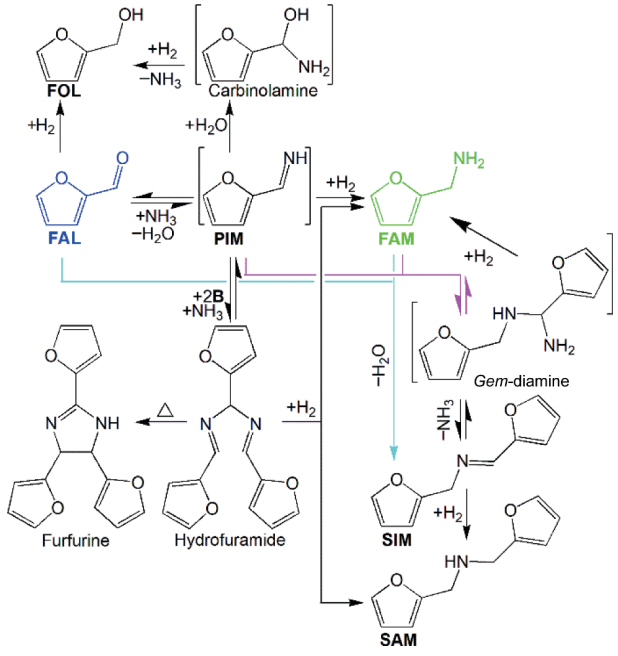

Scheme 1 The reaction route for reductive amination of furfural to furfurylamine: from FAL, PIM, FAM, FOL, SIM to SAM.

$Ru/Nb_2O_5{\cdot}nH_2O$ reduced at 300 °C ($Ru/Nb_2O_5{\cdot}nH_2O$-300) is much more than that on $Ru/Nb_2O_5{\cdot}nH_2O$ at 400 °C ($Ru/Nb_2O_5{\cdot}nH_2O$-400). Thus they considered the reason for the difference in activity of these catalysts may be due to their difference in acidity [31]. Zhang et al. reported a highly efficient and robust Ru/ZrO_2 catalyst which gave an ethanolamine yield as high as 93% in the reduction amination of glycolaldehyde when it was reduced at 150 °C (Ru/ZrO_2-150). They found that Ru states and the acidic sites could be adjusted by reduction temperature. RuO_2 worked as acidic promoter to facilitate the activation of carbonyl groups, while metallic Ru works as active sites for imine hydrogenation, the cooperation between these two types of active sites contributed to the excellent performance of Ru/ZrO_2-150 [32]. Ding et al. suggested that the dispersion of Ru nanoparticles (NPs) (at a range of 8.7%–24.7%) had a negligible effect but the acid sites influenced the reductive amination of furfural over the Ru/HZSM-5 catalysts remarkedly, the Ru/HZSM-5(46) containing optimized acid sites and interaction of metal–support presented the optimum performance with a yield of 76% to FAM [33]. While, Wang et al. found the Ru dispersion influenced the reductive amination of cyclopentanone to cyclopentylamine over Ru/Nb_2O_5 catalyst with different morphologies (layer, hollow, flower-like), cyclopentylamine was produced with a yield of 84.3% [34]. Besides, Hara et al. reported that the structure or the morphology could also affect the catalytic performance, the one of face-centered-cubic (fcc) Ru NPs catalyst with rich {111} facets exposed on the flat Ru particles showed superior catalytic performance for the reduction amination of FAL to FAM (yield of 99%) [35]. For the reduction amination of carbonyl compounds to primary amines, the synergistic or cooperating effects among several factors should exist and contribute to the catalytic performances. For example, Nishimura et al. proposed that the catalytic activity depended on the Ru nanoparticle size and the state of Ru species (RuO_2/Ru) on Ru supported BEA catalysts [36]. Han et al. reported the acidity, the reduction degree of RuO_2, and the electronic density of Ru species were the important factors to influence the performance of reductive amination over Ru/TiP catalyst [37]. Zhang et al. prepared a Ru_1/NC-900-800NH_3 catalyst with Ru single atom dispersed and revealed that a blocked Lewis pair formed between the Ru metal center with high electron density and N atom was conducive to the H_2 dissociation in a heterolytic manner, thus promoting the reductive amination of FAL to FAM [38].

Pd, Rh, Ru noble metal catalysts have been widely studied in reductive amination for their superior activity in hydrogenation. However, the high price and the limited resource restrict their utilization, thus, non-precious metallic Ni- [28, 39–55] and Co-catalysts [27, 28, 47, 55–64] as replacement have attracted more and more attention. It was reported that the identity of the metal is known to have a strong effect on the selectivity to primary amines, with an improving order of Pt < Pd < Rh < Ru < Ni < Co [27, 28]. Ding et al. reported an efficient $10Ni/Al_2O_3$ catalyst, it exhibited a high reaction rate of 23.5 h^{-1} and the high yield to FAM (> 99%), however, FAM could be further hydrogenated to tetrahydrofurfury-amine during the reaction. The strong metal–support interaction, suitable acid sites, and good Ni dispersion guaranteed the outstanding performances of the Ni/Al_2O_3 catalyst [51]. Hara et al. also reported the synergistic effect of small metallic Ni and metal oxide NiO nanoparticle endowed the carbon modified Ni@dendritic silica catalyst to show high activity and high selectivity in the reductive amination of FAL to FAM [54]. However, compared to the noble metals the activitives of Ni and Co are lower (Table S1 in the Electronic Supplementary Material (ESM)), it remains big challenge in designing efficient catalyst with non-noble metals.

Herein, we report an efficient Ni/SiO_2 catalyst for reductive amination of FAL to FAM in the presence of NH_3 and H_2, with it FAM was produced with a high yield around 98%. The Ni/SiO_2 catalysts were prepared by deposition-precipitation or impregnation methods. The structures or the surface properties of catalysts were adjusted by varying Ni loading (7.5%–30%), and calcination temperature (350–550 °C). The catalysts were well characterized by transmission electron microscopy (TEM), high-resolution TEM (HRTEM), scanning TEM (STEM), X-ray diffraction (XRD), H_2-TPR (TPR: temperature programmed reduction), H_2-TPD (TPD: temperature programmed desorption), NH_3-TPD, Fourier transform infrared (FT-IR) spectra of pyridine, and FT-IR spectra of CO adsorption. The relation between the structure and the catalytic performances as well as the reaction route has been discussed. To figure out the reaction pathway and thus control/restrict the products, several control reactions such as transformation of furfural to trimer, hydrogenation of trimer, and the hydrogenation of dimer were examined. This work showed a perspective for the Ni catalyst and provided a useful information for the catalytic reductive amination of carbonyl compounds.

2 Experimental

2.1 Materials

$Ni(NO_3)_2{\cdot}6H_2O$ (Alfa Aesar), Na_2CO_3 (Beijing chemicals), SiO_2 (Aladdin, 50 nm, denoted as SiO_2-I), SiO_2 (Aldrich, 15 nm, denoted as SiO_2-II), ethanol (XL; AR), tert-butanol (TCI; 99%), furfural (Acros; > 97%), furfuryl amine (TCI; > 98%), furfuryl alcohol (Alfa; > 98%), and chlorobenzene (TCI; 99%) were used as received without further purification. H_2 with a purity of > 99.999% was purchased from Changchun Juyang Gas Co., Ltd.

2.2 Catalyst preparation

The catalyst was prepared by deposition-precipitation and impregnation method, respectively. In a typical deposition-precipitation method, 2 g SiO_2-I was added to 100 mL distilled water in a three-necked flask, and then stirred for 0.5 h until SiO_2 was uniform dispersed. After that, the aqueous solution of $Ni(NO_3)_2{\cdot}6H_2O$ (1 M) and Na_2CO_3 (1.5 M) with a Na_2CO_3/Ni

molar ratio of 1.5 was simultaneously dripped to the slurry under stirring at a rate of 60 mL·h^{-1} at 35 °C, then the resulted slurry solution was stirred at 55 °C for 1 h. The resulted precipitate was washed with distilled water until its surface reached neutral with pH indicator strip, then dried at 90 °C and calcinated in air flow at 450 °C for 2 h, and reduced with H_2 flow at 580 °C for 2 h. The final sample was denoted as Ni/SiO_2-I-DP. The Ni loading in weight was about 15%, DP referred to deposition-precipitation method. SiO_2-II supported Ni prepared as above method was denoted as Ni/SiO_2-II-DP. For comparison, a similar catalyst was prepared by equal volume impregnation method, the sample were dried overnight at 90 °C. The following thermal treatments were the same as the above described. The obtained catalyst was named as Ni/SiO_2-I-IM, IM referred to impregnation method. For the catalyst without special instructions, the loading amount was 15%, and the calcination temperature was 450 °C.

2.3 Catalyst characterization

Powder XRD (PXRD) patterns of reduced catalysts were measured on a Bruker D8 Advance X-ray powder diffraction instrument with a Cu-Kα radiation (λ = 0.154 nm) in the 2θ range of 20°–80° with a scan speed of 4°·min^{-1}. TEM and HRTEM observations were performed on a field emission JEOL JEM-2010 instrument at 200 kV. The STEM images were obtained with an energy dispersive spectroscopy (EDS) detector, by Tecnai G2 TEM operating at 200 kV. The reduced samples were ultrasonically dispersed in ethanol before deposited on the double-linked copper mesh. H_2-TPR, H_2-TPD, and NH_3-TPD experiments were performed on a Micromeritics Autochem II 2920 chemisorption instrument equipped with a thermal conductivity detector (TCD). In a typical H_2-TPR experiment, the sample was pretreated in Ar atmosphere at 150 °C for 1 h to remove physically adsorbed H_2O and other impurities. After cooling to 50 °C, the sample was measured by heating from 50 to 900 °C with a ramping rate of 10 °C·min^{-1} in a 5% H_2/Ar flow (50 cm^3·min^{-1}). In a typical H_2-TPD experiment, the sample was *in situ* reduced for 2 h at 580 °C in a 5% H_2/Ar flow. After cooling to 50 °C, purging with Ar to remove physically adsorbed hydrogen until the baseline reached stable, the sample was measured in an Ar flow (50 cm^3·min^{-1}) at a temperature range of 50–900 °C with a heating rate of 10 °C·min^{-1}. In a typical NH_3-TPD experiment, the sample was *in situ* reduced for 2 h at 580 °C. After cooling to room temperature, the sample adsorbed ammonia for 0.5 h, then the sample was heated in helium (He) atmosphere at 100 °C for 0.5 h to remove physically adsorbed NH_3. After that, the sample was cooled to room temperature and measured from room temperature to 900 °C at a heating rate of 10 °C·min^{-1} in He flow (50 cm^3·min^{-1}). The contents of Ni in the Ni/SiO_2 catalysts were obtained by inductively coupled plasma (ICP) on Thermo Scientific X series II, the actual Ni loadings were close to the theoretical ones. X-ray photoelectron spectroscopy (XPS) measurements were performed on VG Microtech 3000 Multilab. Nitrogen sorption isotherms were measured at −196 °C by using a Micromeritics ASAP 2020 instrument after degassing the samples under vacuum at 300 °C for 10 h. The surface areas were calculated by the Brunauer–Emmett–Teller (BET) method. The relative concentration of Brønsted and Lewis acid sites was measured by infrared spectroscopy (Vertex 70, Bruker) of adsorbed pyridine. The sample was pressed into a disc (diameter of 13 mm) and it was reduced under H_2 at 580 °C for 2 h and cooled down to room temperature, followed by the collection of the background of the IR spectrum. Next, the temperature was increased from room temperature to 130 °C; the sample was kept in pyridine vapor for 0.5 h, and then the sample was kept in flowing He at 200 °C for 0.5 h to allow the physiosorbed pyridine to desorb. Afterwards, the sample was cooled to ambient temperature. Then, the FT-IR spectrum was collected at a range of wavelengths from 400 to 4,000 cm^{-1}. Diffuse reflectance infrared Fourier transform (DRIFT) spectra of CO adsorption and secondary imine (SIM) adsorption were examined on a Thermo Scientific Nicolet iS50 spectrometer equipped with a mercury cadmium telluride (MCT) detector. The sample was reduced under H_2 at 580 °C for 2 h and cooled down to room temperature, then the sample was purged by flowing He at 70 mL·min^{-1} for 10 min at 30 °C. Then, the background was recorded. For CO adsorption, the sample was exposed to a stream of 5% CO/He (70 mL·min^{-1}) for 30 min. The spectra were recorded once per minute while passing He at 70 mL·min^{-1}. For SIM adsorption, after the dripping of 10 μL SIM, the spectra were recorded once per minute while passing He at 70 mL·min^{-1}. Thermogravimetric analysis (TGA) was obtained on TA-Q50 instruments. The sample was heated from 50 to 800 °C at a heating rate of 10 °C·min^{-1} in a N_2 flow.

2.4 Reductive amination of furfural

The catalytic performance of Ni/SiO_2 catalysts in the reductive amination of furfural was performed in a 50 mL stainless steel autoclave. The catalyst was pre-reduced in a quartz tube at 580 °C in a H_2 flow for 2 h. After reduction finished, the catalyst was cooled to room temperature and purged with N_2 for 0.5 h. Then the catalyst was immediately transferred to the reactor containing a mixture of 5 mmol furfural reactant and 5 mL tert-butanol solvent, the reactor was flushed with H_2 five times to remove the air and placed in a water bath waiting for about 10 min to warm up it to 90 °C. Then, NH_3 (0.8 MPa) and H_2 (4 MPa) were introduced into the reactor in sequence, and the reaction was started with a stirring rate of 1,300 rpm. After the reaction finished, the autoclave was cooled down in ice-water and then depressurized slowly. After the suspension was centrifugated and separated, the liquid products were analyzed by gas chromatography (GC, Shimadzu, GC-2014) equipped with a capillary column (Restek Stabilwax 30 m × 0.53 mm × 1 μm) and a flame ionization detector (FID). All liquid products were identified by gas chromatography/mass spectrometry (GC/MS, Agilent 5890). Conversion of FAL and yield to products were determined by GC using chlorobenzene as an external standard. The conversion and yield were calculated by the following equations

$$\text{Conversion}\,(\text{mol}\%) = \frac{\text{Mole of furfural consumed}}{\text{Mole of furfural added initially}} \times 100\%$$

$$\text{Yield}(\%) = \left(\frac{\text{Carbon atoms in a certain product produced}}{\text{Carbon atoms of furfural added into reactor}}\right) \times 100\%$$

For the recycling experiment, after reaction the catalyst was collected by centrifugation and washed with ethanol for 5 times, dried at 90 °C for 5 h and reduced at 580 °C for 2 h, then it was used again with adding fresh FAL and solvent together to the reactor.

3 Results and discussion

A series of Ni/SiO_2 catalysts were prepared by different methods and thermal treatments in order to figure out the relation of surface property and structure with the catalytic performance. Three selected catalysts of Ni/SiO_2-I-DP, Ni/SiO_2-II-DP, and Ni/SiO_2-I-IM as described in Section 2 were mainly characterized and studied for the reductive amination of FAL. The effects of the morphology and structure of the Ni nanoparticles on the catalytic performance were discussed in detail.

3.1 Structure and properties

At first the morphology and the Ni nanoparticle dispersion on the surface of SiO_2 supports were examined by TEM measurement. As the images shown in Fig. 1, the catalysts Ni/SiO_2-I-DP and Ni/SiO_2-II-DP prepared by deposition-precipitation presented a homogeneous dispersion of Ni in a particle size around 3 nm, irrespective to the kind of support used, and it is also observed from the elemental mapping images that Ni is highly dispersed on the surface of SiO_2 (Fig. S1 in the Electronic Supplementay Material (ESM)). While, by comparison, Ni/SiO_2-I-IM prepared by impregnation showed a serious aggregation of Ni particles, the average size of Ni particles is around 18 nm, indicating the preparation method has a significant influence on the Ni dispersion. It is interesting, the morphology of the Ni nanoparticles was different on the Ni/SiO_2-I-DP and Ni/SiO_2-II-DP, although the same of Ni dispersion on them. As seen in Fig. 2, the flat-shaped Ni particles showed on the surface of Ni/SiO_2-I-DP (Fig. 2(a)) but such flat-shaped Ni particles were hardly observed on Ni/SiO_2-II-DP, instead of that the particle in a kind of ideal sphere clearly presented (Fig. 2(b)). Besides, the Ni/SiO_2-I-DP prepared with different Ni loading was also examined, and it was found a big difference in Ni dispersion (Fig. S2 in the ESM), at high Ni loading the Ni particle aggregated largely. However, the thermal treatment at a calcination temperature range of 350–550 °C showed very slight effect on the Ni dispersion, all the Ni particle size is around 3 nm (Fig. S3 in the ESM).

The XRD patterns also demonstrated the similar results for the Ni/SiO_2-I-DP, Ni/SiO_2-II-DP, and Ni/SiO_2-I-IM catalysts (Fig. 3). The diffraction patterns attributing to Ni(111), Ni(200), and Ni(220) were detected for all the samples, similar to the crystal planes measured on the TEM images. It is broadened and weak for Ni/SiO_2-I-DP and Ni/SiO_2-II-DP, but sharp on Ni/SiO_2-I-IM, demonstrating again that the particle sizes of Ni on Ni/SiO_2-I-DP and Ni/SiO_2-II-DP are small with a uniformly dispersion. By contrast, the Ni particles aggregated significantly on the surface of Ni/SiO_2-I-IM. It was reported that a $Ni_3Si_2O_5(OH)_4$ phase was formed under the alkaline conditions during deposition-precipitation preparation [65], the formation of $Ni_3Si_2O_5(OH)_4$ resulted in the uniform dispersion of Ni on SiO_2 as the stronger interaction between Ni and the support. For the Ni/SiO_2-I-DP catalysts with different Ni loadings (Fig. S4 in the ESM), the results of XRD were consistent with those of TEM results.

In addition, the reduction behavior of the catalysts was examined by TPR analysis, the results are shown in Fig. 4. The reduction behaviors largely depended on the preparation method, for the catalyst prepared by deposition-precipitation of Ni/SiO_2-I-DP and Ni/SiO_2-II-DP, they presented the similar reduction peaks at 558 and 632 °C. By contrast, the Ni/SiO_2-I-IM prepared by impregnation presented the reduction peak at the lower temperatures of 305–364 °C. The difference in the reduction temperature of NiO in the samples should be ascribed to the strength of the interactions of NiO with SiO_2. The reduction degree of NiO in Ni/SiO_2-I-DP and Ni/SiO_2-I-IM was similar, but the amount of the desorption of hydrogen on the former one was much larger than that on the latter one (Fig. S5 in the ESM and Table 1 entries 1 and 3), indicating the former one with smaller Ni particle has more adsorption/active sites for hydrogen. The reduction degree of NiO in Ni/SiO_2-I-DP was higher than that in Ni/SiO_2-II-DP, but the amount of hydrogen desorption on both the catalysts was similar (Table 1 entries 1 and 2), suggesting the similar amount of active sites for H_2 dissociation on the both catalysts.

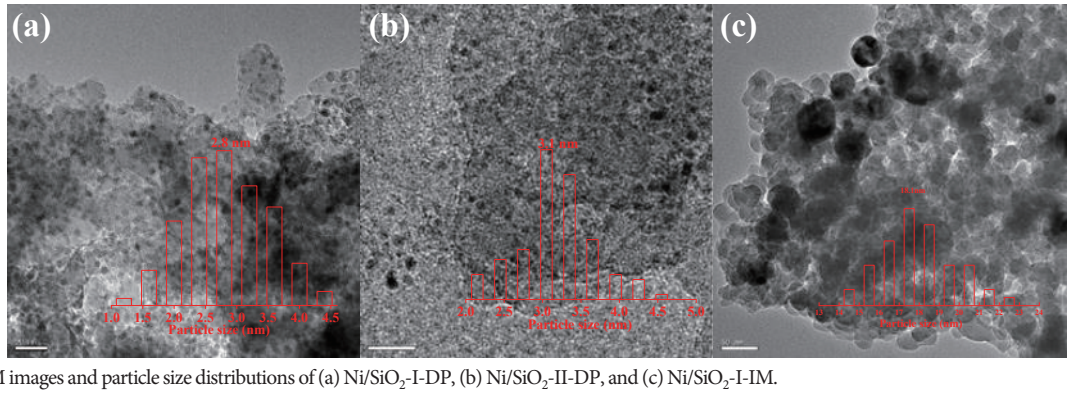

Figure 1 TEM images and particle size distributions of (a) Ni/SiO_2-I-DP, (b) Ni/SiO_2-II-DP, and (c) Ni/SiO_2-I-IM.

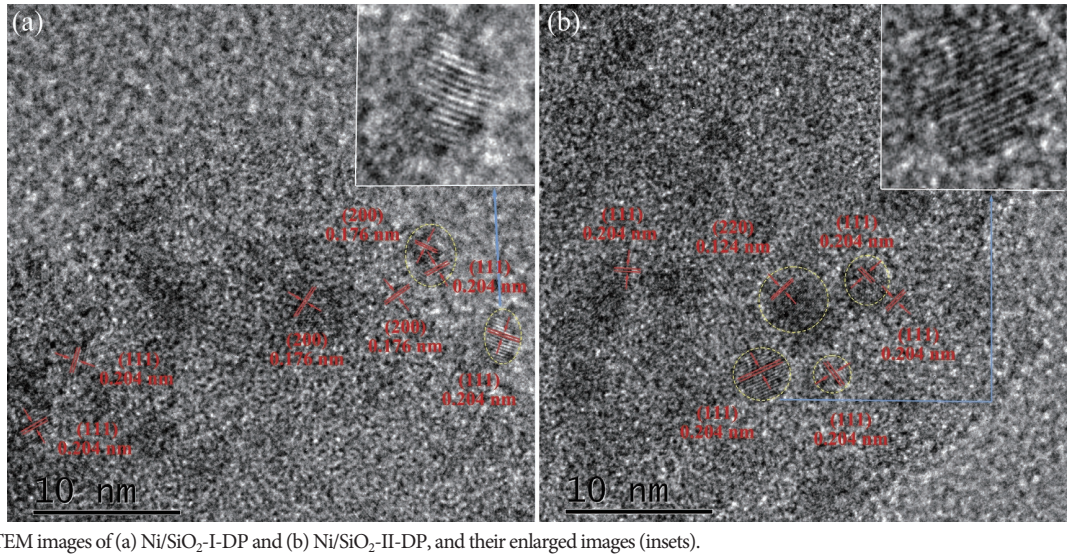

Figure 2 HRTEM images of (a) Ni/SiO_2-I-DP and (b) Ni/SiO_2-II-DP, and their enlarged images (insets).

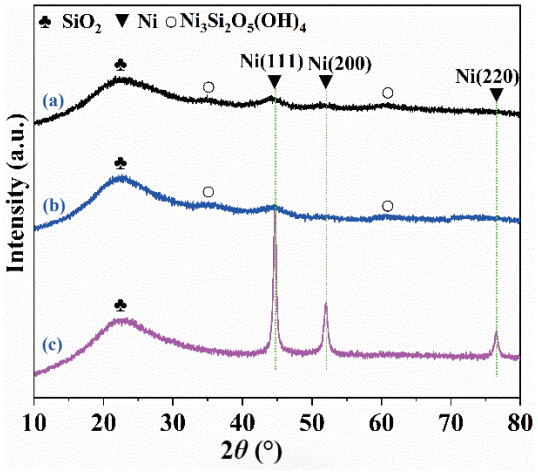

Figure 3 XRD patterns of (a) Ni/SiO_2-I-DP, (b) Ni/SiO_2-II-DP, and (c) Ni/SiO_2-I-IM.

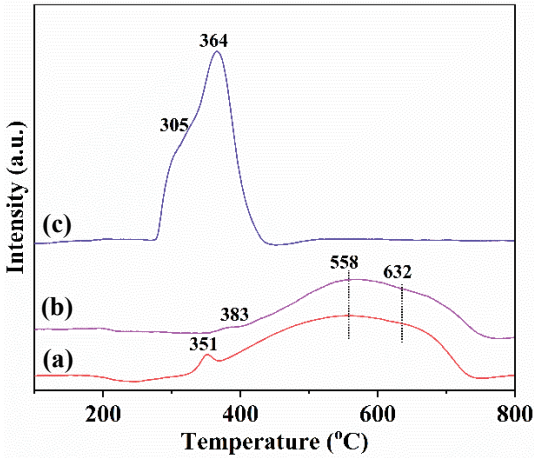

Figure 4 H_2-TPR profiles of Ni/SiO_2 catalysts. (a) Ni/SiO_2-I-DP, (b) Ni/SiO_2-II-DP, and (c) Ni/SiO_2-I-IM. The sample before reduction was used for H_2-TPR test.

Besides, the acidity of the selected catalysts was characterized. The results show that the acidity depended on the sort of support used largely, Ni/SiO_2-I-DP and Ni/SiO_2-I-IM presented the equal amount of acid sites, but Ni/SiO_2-II-DP showed less amount of acidity on its surface (Fig. S6 in the ESM and Table 1). The acidity of the catalyst should mainly come from the support rather than the surface Ni species. Furthermore, the type and concentration of acid sites were examined via FT-IR measurement by adsorbing pyridine, the results are shown in Fig. 5. It was found there are two kinds of Lewis and Brönsted acid sites on the surface of the catalysts checked, and it depended on the supports used also. The similar amount of Lewis and Brönsted acid sites presented on Ni/SiO_2-I-DP and Ni/SiO_2-I-IM. In contrast, the amount of Lewis acid sites of Ni/SiO_2-I-DP is much more than that of Ni/SiO_2-II-DP and the number of Brönsted acid sites is similar on both catalysts, while there are more Lewis acid sites than Brönsted acid sites on these catalysts. It concluded that the surface acidity of Ni/SiO_2 catalysts is mainly coming from the support, irrespective to the presence of Ni species or not.

Moreover, DRIFT spectra of the CO adsorption were also checked. As depicted in Fig. 6 and Fig. S7 in the ESM, the band at 2,181 cm^{-1} corresponds to Ni^{2+}–CO species for Ni/SiO_2-I-IM [66–68], and the broad band with the center of 2,008–2,031 cm^{-1} belongs to the linear CO species adsorbed the edge Ni^0, while that at 1,890 cm^{-1} is assigned to bridge CO adsorption on Ni atoms. Another peak around 1,812 cm^{-1} can be assigned to CO bonded to up to four Ni atoms [66–72]. From Ni/SiO_2-I-IM, Ni/SiO_2-II-DP to Ni/SiO_2-I-DP, the adsorbed band of CO red-shifts from 1,890 to 1,812 cm^{-1}, indicating the Ni terrace/step sites is getting larger and larger [66–68]. The red-shift of CO absorbance peak could be ascribed to the geometric effect as described above but not the electron denoting effect as reported on Ru/Nb_2O_5 and Ru/TiP [26, 37], because the electronic state of Ni^0 is similar in all Ni/SiO_2 catalyst (Fig. S8 in the ESM). The results of CO adsorption are consistent with that observed from HRTEM analysis, that the flat-shape Ni has the larger Ni step on the Ni/SiO_2-I-DP compared with the spherical-shape Ni on the Ni/SiO_2-II-DP, the former one is beneficial to the adsorption of CO on multiple Ni. In addition, the intensity of the bridge CO adsorption is in an order of Ni/SiO_2-I-DP > Ni/SiO_2-II-DP > Ni/SiO_2-I-IM, which is also the order of the amount of the large Ni step on these catalysts. Ni/SiO_2-I-DP has the largest step surface, and this kind of step surface is the most in amount.

3.2 Relation of structure and catalytic performance

The catalytic performance of the selected catalysts of Ni/SiO_2-I-DP, Ni/SiO_2-II-DP, and Ni/SiO_2-I-IM was evaluated for the reductive amination of FAL, and the relationship of the structure and activity/selectivity has been discussed. In the reductive amination of FAL, several reaction steps are included as shown in Scheme 1. At first, the condensation of FAL with ammonia could occur and generated corresponding primary imine (PIM), an intermediate, which is unstable and difficult to detect or isolate from the reaction mixture. In the presence of a catalyst, PIM could be hydrogenated to the desired product of FAM. Then FAM was further condensed with FAL to form SIM as the nucleophilic addition activity of FAM is much higher than NH_3 [73]. Therefore, once FAM was formed, it would condense with FAL or PIM to form SIM. In the presence of excess NH_3, the existing form of SIM should be *gem*-diamine, although *gem*-diamine is unstable and difficult to detect. *Gem*-diamine was then

Table 1 Physical and chemical properties of catalysts

Entry	Catalyst	Particle size (nm)[a]		H_2 consumption ($cm^3 \cdot g^{-1}$)[b,c]	Reduction degree (%)[d]	H_2-TPD ($cm^3 \cdot g^{-1}$)[b,e]	NH_3-TPD ($cm^3 \cdot g^{-1}$)[b,f]	Acid site ($\mu mol \cdot g^{-1}$)[g]		S_{BET} ($m^2 \cdot g^{-1}$)[h]	Pore volume ($cm^3 \cdot g^{-1}$)[h]	Pore diameter (nm)[h]
		TEM	XRD					B	L			
1	Ni/SiO_2-I-DP	2.8	—	38.8	67.7	3.5	6.0	39.0	245.3	213	1.00	3.06
2	Ni/SiO_2-II-DP	3.1	—	29.9	52.1	3.1	3.0	34.8	133.5	321	0.96	6.55
3	Ni/SiO_2-I-IM	18.1	15.1	40.3	70.3	0.3	6.0	38.2	244.4	176	1.32	3.06

For all the catalyst examined, Ni loading is 15%, all the samples were calcined at 450 °C. [a]Average size of the Ni nanoparticles was determined by TEM (Fig. 1) and XRD analyses (Fig. 3), respectively. [b]The dosage of samples used is 0.1 g. [c]The H_2 consumption of the unreduced catalysts was determined by H_2-TPR measurement. The temperature was raised from 30 to 580 °C at 10 °C·min^{-1} and maintained at 580 °C for 2 h. [d]The reduction degree of the catalyst was obtained by the ratio of the hydrogen consumption measured by H_2-TPR to the theoretical one. The theoretical hydrogen consumption of the catalyst was 57.3 $cm^3 \cdot g^{-1}$ as calculated based on the complete reduction of NiO to metallic Ni. [e]The amount of H_2 desorption (Fig. S5 in the ESM). [f]The amount of NH_3 desorption (Fig. S6 in the ESM). [g]The amount of Brönsted (B) and Lewis (L) acid were calculated based on pyridine adsorption by FT-IR spectra (Fig. 5). [h]S_{BET} is BET surface area, the pore volume was estimated by the Barrett–Joyner–Halenda method, and the pore diameter was determined by the density functional theory method.

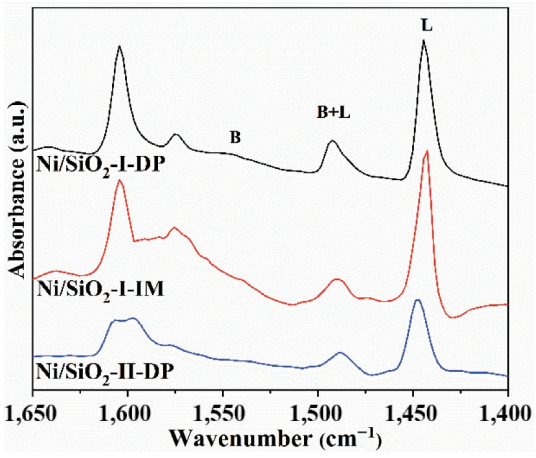

Figure 5 FT-IR spectra for pyridine adsorbed on different catalysts.

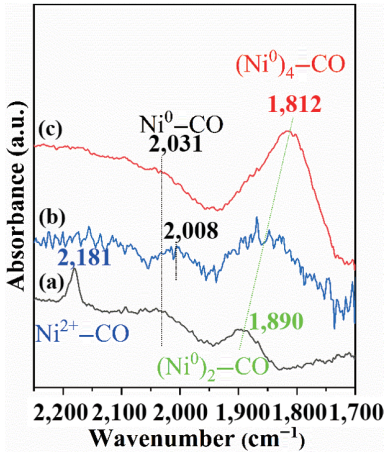

Figure 6 DRIFT spectra of CO adsorption on (a) Ni/SiO_2-I-IM, (b) Ni/SiO_2-II-DP, and (c) Ni/SiO_2-I-DP at 30 °C after CO adsorption and purging with He for 10 min (Fig. S7 in the ESM).

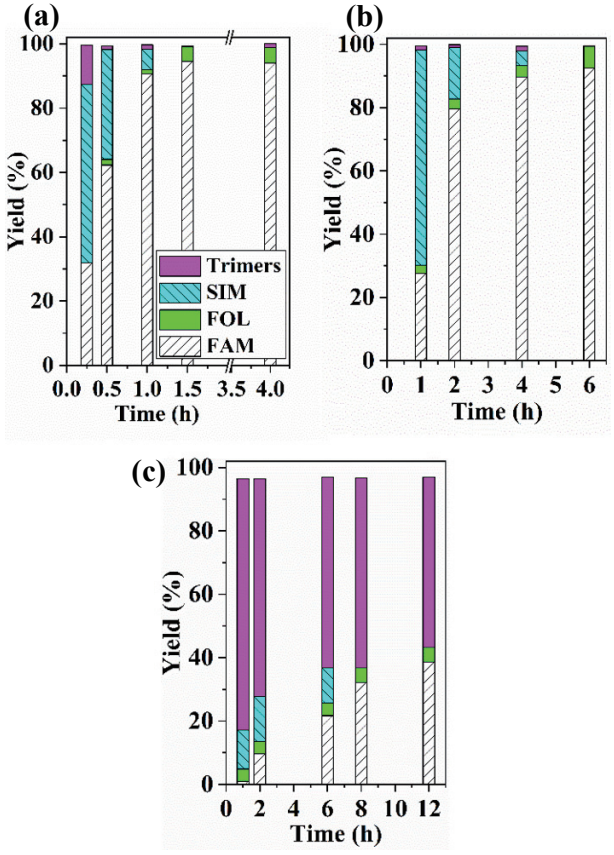

Figure 7 Time–yield profiles of reductive amination of furfural over (a) Ni/SiO_2-I-DP, (b) Ni/SiO_2-II-DP, and (c) Ni/SiO_2-I-IM. Reaction conditions: 5 mmol furfural, 5 mL *tert*-butanol, 0.1 g catalyst, 0.8 MPa NH_3, 4 Mpa H_2, and 90 °C. It is noted the conversion exceeded over 99.9% on all catalysts.

hydrogenated to FAM directly or reversibly converted to FAM and PIM, which are then hydrogenated to FAM. If the catalyst was less selective, the direct hydrogenation of FAL to furfuralcohol (FOL) and the hydrogenolysis of PIM to FOL would also occur. Moreover, the intermediate of SIM could be further hydrogenated to give secondary amine (SAM). When the hydrogenation of PIM is quite slow, the accumulation of PIM and side reactions would occur [26]. PIM can be trimerized to form hydrofuramide, which subsequently undergoes thermal cyclization to give furfurine. Hydrofuramide could be transformed to FAM also, but furfurine could not [26, 74].

The results of the reduction amination of FAL are shown in Fig. 7. For the Ni/SiO_2-I-DP and Ni/SiO_2-II-DP catalysts, SIM was mainly produced as an intermediate in the initial stage of the reaction, and then it transformed to FAM with extending reaction time (Fig. 7). Over Ni/SiO_2-I-DP catalyst, FAM was produced with a maximum of 94.6% within 1.5 h, and the value changed slightly with further hydrogenation up to 4 h, the deep hydrogenation product of tetrahydrofurfurylamine was not observed (Fig. 7(a)). While, on the Ni/SiO_2-II-DP, the transformation of SIM is much slower, to reach the maximum yield of FAM (92.5%) needed 6 h (Fig. 7(b)). Moreover, Ni/SiO_2-I-IM showed largely difference to the above two catalysts, with it trimers of hydrofuramide and furfurine was produced at the initial stage of reaction, and hydrofuramide slowly generated to FAM, the maximum yield of FAM (38.6%) obtained at 12 h was much lower (Fig. 7(c)). The conversion of FAL can reached 100% over all catalysts, the formation of FAM depended on the rate of intermediate SIM formation (Table 2), which is closely related to the particle size of the catalyst (Fig. 8). The small Ni particle size could provide more active sites for the activation and dissociation of hydrogen, and thus promoted the hydrogenation reaction resulting in the formation of SIM and then FAM, however, it is not the smallest, the best. For example, the Ni/SiO_2-I-DP prepared with a 7.5% Ni loading had a smaller Ni particle size of 2.1 nm, on which the yield of FAM was 87.1%, which is a little lower than that on the catalyst with a 15% Ni loading and a bigger Ni particle size of 2.8 nm, due to more FOL was formed on the former one (Table 2 entries 1 and 2). For Ni/SiO_2-I-DP and Ni/SiO_2-II-DP having similar Ni particle in size (~ 3 nm), they exhibited similar yield to FAM (92%–95%). But the forming rate of FAM on Ni/SiO_2-I-DP is much higher than that on Ni/SiO_2-II-DP (Table 2 entries 3 and 5). One possible reason might come from the acidity, the amount of Lewis acid sites is much more on the former compared to the latter one. The Lewis acid sites could profit the adsorption and the hydrogenation of PIM and *gem*-diamine to FAM. Although Ni/SiO_2-I-DP and Ni/SiO_2-II-DP have certain differences in acidity, their acidity is relatively weak and SiO_2 is generally a neutral or inert carrier. Thus, except for the acidity the morphology or the atomic stacking structure of Ni particles on the Ni/SiO_2 catalysts examined herein should be considered. The flat-shaped Ni with the large and multiple step surface on the Ni/SiO_2-I-DP may favor the adsorption of PIM and *gem*-diamine by horizontal adsorption mode, benefiting the formation of FAM, which is in agreement to the results in literature, in which the flat-shape catalyst was suggested to be beneficial to the reductive amination of carbonyl compounds [35, 62]. Hara et al. has reported the catalytic performance of the flat-shaped fcc Ru NPs was much better than that spherical-shape hexagonal-close-packed structure of Ru NPs because fcc Ru NPs could be able to generate a large fraction of open {111} facets with the large fraction of

Table 2 The results of reductive amination of FAL over different Ni/ SiO_2 catalysts[a]

Entry	Catalyst	Ni loading (%)	Calcination temperature (°C)	Particle size (nm)	Time (h)	Yield (%)					Rate (h^{-1})[c]
						FAM	FOL	SIM	Trimers	Others[b]	
1	Ni/SiO_2-I-DP[d]	7.5	450	2.1	1	87.1	12.0	1.0	—	—	17.0
2	Ni/SiO_2-I-DP	15	450	2.8	1	90.7	1.3	6.3	1.4	0.2	17.7
3	Ni/SiO_2-I-DP	15	450	2.8	1.5	94.6	4.4	—	0.3	0.7	12.3
4	Ni/SiO_2-I-DP	15	550	3.0	1.5	91.2	6.3	—	0.1	0.3	11.9
5	Ni/SiO_2-II-DP	15	450	3.1	6	92.5	6.9	—	0.2	0.4	3.0
6	Ni/SiO_2-I-DP	15	350	3.7	1.5	91.5	7.2	—	0.1	1.2	11.9
7	Ni/SiO_2-I-DP[e]	30	450	7.8	8	63.4	0.6	—	34.6	1.4	1.6
8	Ni/SiO_2-I-IM	15	450	18.1	8	32.2	4.5	—	60.1	3.2	0.8
9	Raney Ni[f]	—	—	13.6	24	75.7	0	4.5	19.7	0.1	0.6

Reaction conditions: 5 mmol furfural, 5 mL *tert*-butanol, 0.1 g catalyst, 0.8 MPa NH_3, 4 MPa H_2, and 90 °C. [a]The data were collected just when the SIM was completely converted, [b]uncertain products, [c]rate was calculated by per mole of FAM produced per mole Ni per hour, [d]0.2 g, [e]0.05 g, and [f]0.015 g.

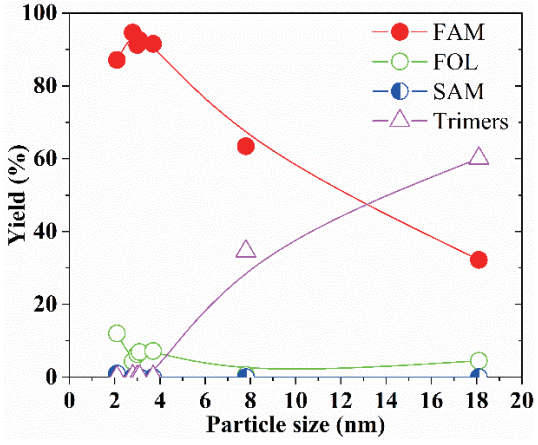

Figure 8 The yield to furfuryl amine as a function of Ni particle size.

metallic Ru [35]. Mitsudome et al. has reported that the performance of Co_2P nanorods (Co_2P NRs) was better than that of the bulk Co_2P, CoP nanoparticles sponge Co, and Co/SiO_2 for the reduction amination of benzaldehyde to benzylamine [62]. For Ni/SiO_2-I-IM, the particle size of Ni is larger, its ability to activate hydrogen is relatively poor (Table 1 entry 3), in this case PIM was easily transformed into trimers, resulting in low yield of FAM (Table 2 entry 8). The amount of acid sites of Ni/SiO_2-I-IM is equal to that of Ni/SiO_2-I-DP, but the amount of the Ni step surface of Ni/SiO_2-I-IM was much less than that of Ni/SiO_2-I-DP (Fig. 6). It suggested again that the structure of Ni particles played an important role, the smaller Ni particle with flat steps is conductive to the activation of hydrogen and the horizontal adsorption of intermediates (PIM and *gem*-diamine), favoring the hydrogenation of intermediates to FAM. That was also demonstrated by a series catalyst of Ni/SiO_2-I-DP calcined at a range of temperatures (350–550 °C). The difference in calcinating temperature did not change the Ni particle size, the surface species ratio Ni^0/NiO, the hydrogen adsorption as well as the surface acidity (Table S2 entries 1, 3 and 4 in the ESM), thus FAM was formed with the similar rate on these catalysts (Table 2 entries 3, 4 and 6). As analysis of the surface properties of the catalysts listed in Table S2 and Fig. S8 in the ESM, the effects of the surface area of catalysts and the electronic state of Ni could be excluded. Moreover, the one of Ni/SiO_2-I-DP (30% Ni), having a Ni particle of 7.8 nm, exhibited a lower forming rate of FAM (Table 2 entry 7). It is to note that the yield to FAM (94.6%) and its formation rate (12.3 h^{-1}) over Ni/SiO_2-I-DP were much higher than these on Raney Ni (75.7% and 0.6 h^{-1}) (Table 2 entries 3 and 9). Overall, the results showed that Ni/SiO_2-I-DP is effective for the present reductive amination reaction. The activity and product selectivity mainly depend on the structure of Ni particle. The smaller Ni particle benefits for the activation of H_2 thus accelerating the hydrogenation reaction steps, the larger and more flat step surface favors the horizontal adsorption of substrate thus promoting the formation of FAM.

3.3 Reaction mechanism

In order to better understand the reaction pathways and mechanism, the adsorption and transformation of SIM were performed and compared for the catalysts selected. DRIFT spectra of the SIM adsorption at 30 °C are shown in Fig. 9. It presented a strong adsorption on the surface of Ni/SiO_2-I-DP after SIM adsorption and purging He for 205 min (Fig. 9(a)). However, the SIM adsorption was not detected on the surface of Ni/SiO_2-II-DP after SIM adsorption with He purging only for 8 min (Fig. 9(b)). The adsorption strength is in an order of Ni/SiO_2-I-DP >> Ni/SiO_2-I-IM > Ni/SiO_2-II-DP based on the desorption rate. The adsorption of SIM is relative with Ni step surface and the surface acidity. Furthermore, the reductive amination of SIM, was carried out and compared among the above three catalysts, the SIM could be converted to FAM almost without hydrogenation to SAM (Fig. 10). The reaction rate of SIM to FAM is in an order of Ni/SiO_2-I-DP > Ni/SiO_2-II-DP > Ni/SiO_2-I-IM, which is related to both the ability of activation of hydrogen (Ni/SiO_2-I-DP ≈ Ni/SiO_2-II-DP >> Ni/SiO_2-I-IM, Table 1) and the adsorption strength (Ni/SiO_2-I-DP >> Ni/SiO_2-I-IM > Ni/SiO_2-II-DP, Fig. 9). For the reductive amination, once FAM was formed, it would condense with FAL to form SIM, or with PIM to form SIM, in the presence of excess NH_3, SIM adsorbed on the surface of Ni formed *gem*-diamine. Activated hydrogen was added to *gem*-diamine to form FAM. Therefore, the ability to activate hydrogen and the adsorption strength of SIM on the catalyst are important for the formation of FAM with high yield.

Besides, the amination of FAL to trimers in the absence and presence of catalyst was also examined, the results are shown in Fig. 11. Without catalyst, FAL could react rapidly with NH_3 to form hydrofuramide, which was easily cyclized to form furfurine. In the presence of Ni/SiO_2, the formation of trimers was inhibited. The forming rate of trimers is in an order of Ni/SiO_2-I-DP < Ni/SiO_2-II-DP < Ni/SiO_2-I-IM at the initial stage. The adsorption mode of PIM by horizontal direction on the larger Ni step surface may be stronger to retard its desorption and the formation of trimers. The reductive amination with trimers as starting reactant was also checked under the same reaction conditions (Fig. 12).

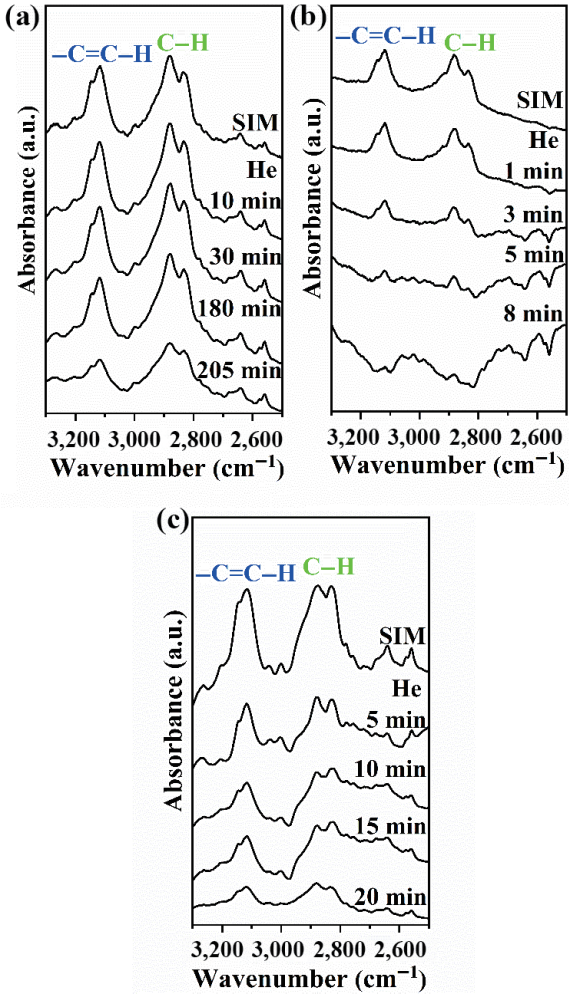

Figure 9 DRIFT spectra of secondary imine adsorption on (a) Ni/SiO_2-I-DP, (b) Ni/SiO_2-II-DP, and (c) Ni/SiO_2-I-IM.

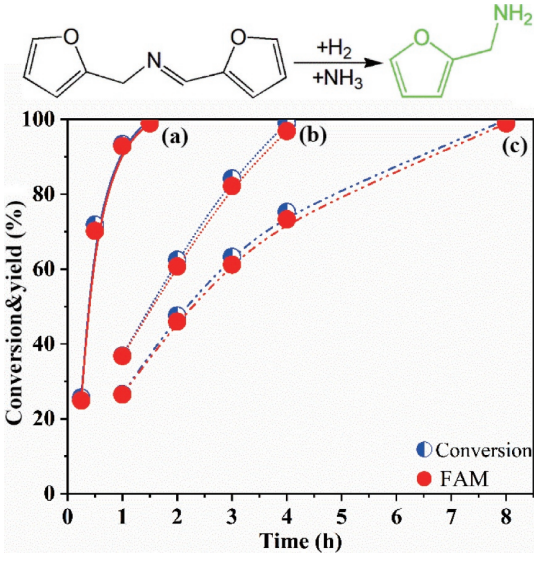

Figure 10 Time–conversion/yield profiles of reductive amination of SIM: (a) Ni/SiO_2-I-DP, (b) Ni/SiO_2-II-DP, and (c) Ni/SiO_2-I-IM. Reaction conditions: 2.5 mmol SIM, 5 mL *tert*-butanol, 0.1 g catalyst, 0.8 MPa NH_3, 4 MPa H_2, and 90 °C.

Trimers were self-synthesized from a reaction of FAL with NH_3, in which the two kinds of trimers of hydrofuramide and furfurine could be formed but they cannot be separated and identified under our chromatographic conditions. Hydrofuramide can be reversibly converted to PIM and then hydrogenated to FAM. Hydrofuramide can be hydrogenated to FAM and SAM [39], the

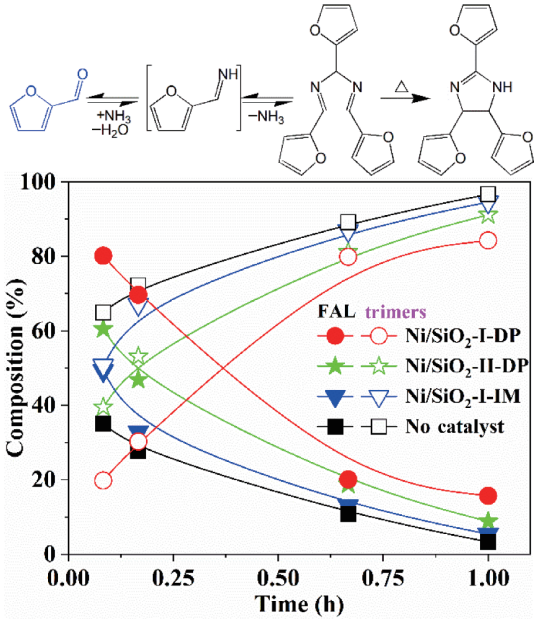

Figure 11 Time–composition profiles of furfural to trimers of hydrofuramide and furfurine. Reaction conditions: 5 mmol furfural, 5 mL *tert*-butanol, 0.1 g catalyst, 0.8 MPa NH_3, and 90 °C.

reaction did not occur over Ni/SiO_2 because SAM was not detected. Furfurine is stable and cannot be further transformed [26, 74]. The conversion of trimers to FAM is much slower than the transformation of FAL or SIM to FAM, and the conversion is below 15%. The results suggested if the hydrogenation activity was low, the trimers formed from the aggregated PIM will be difficult to convert to FAM. Based on the above, the present reductive amination contained several competitive steps. The formation of trimers will lower the production of desired product of FAM; thus, the catalyst should be sufficiently active and selective, the rapid hydrogenation of PIM would reduce its accumulation and thus prevent the side reaction of PIM to trimer.

Finally, the reaction conditions were evaluated, hydrogen pressure showed an influence on the yield to FAM, the highest yield of 97.9% presented at 2 MPa (Fig. 13). The higher hydrogen pressure is beneficial to hydrogenation of PIM and *gem*-diamine to FAM, but too high will promote the hydrogenation of FAL and PIM to FOL. The influence of NH_3 pressure was much significant, the yield to FAM enhanced significantly from 37.9% to 97.9% with increasing NH_3 pressure from 0.4 to 0.8 MPa, while it decreased sharply to 16.7% when NH_3 pressure increased to 1.2 MPa. Increasing NH_3 pressure can inhibit the conversion of PIM to trimers, then promote the formation of FAM. But too high NH_3 pressure causes the hydrogenation active site to be covered by NH_3. The optimum conditions were confirmed to be 90 °C, 2 MPa H_2, 0.8 MPa NH_3, and 1.5 h, at which a high reaction rate of 12.8 h^{-1} was achieved, it is much higher than the results reported on the most non-noble metal catalysts in literature (Table S1 in the ESM). The Ni/SiO_2-I-DP catalyst is also effective for the reductive amination of aldehydes (benzaldehyde and 5-hydroxymethylfurfural) and ketones (cyclohexanone and acetophenone) to their corresponding primary amine with a yield at a range of 85%–93% (Table S3 in the ESM). The Ni/SiO_2-I-DP catalyst could be used for four times with a slightly decrease in the yield to FAM (Fig. S9 in the ESM), which is ascribed to the carbon deposition as confirmed by TGA measurement (Fig. S10 in the ESM). For the recycled catalyst, the agglomeration of Ni particles did not occur (Fig. S11 in the ESM), and Ni leaching was not detected by ICP measurement, the Ni loading on the 4th recycled catalyst is still 15.0%, near to the fresh one (15.1%). With the activity decreasing, the hydrogenation of SIM slowed down,

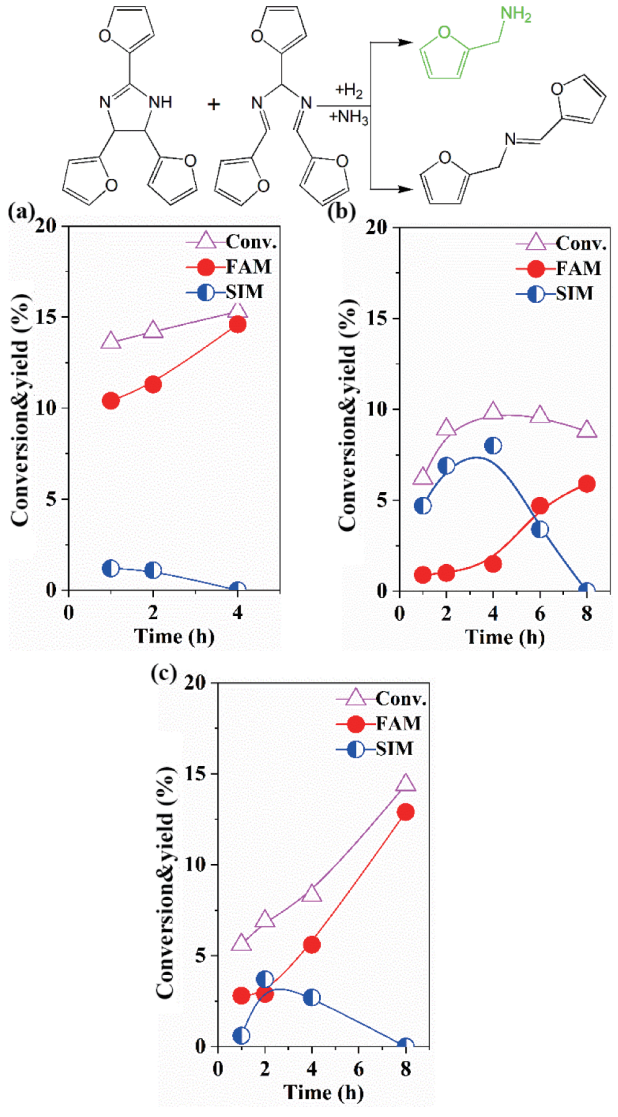

Figure 12 Time–conversion/yield profiles of reductive amination of trimers: (a) Ni/SiO_2-I-DP, (b) Ni/SiO_2-II-DP, and (c) Ni/SiO_2-I-IM. Trimers including hydrofuramide and furfurine were prepared with a 96.7% yield at reaction conditions: 5 mmol furfural, 5 mL *tert*-butanol, 0.8 MPa NH_3, 90 °C, and 1 h without catalyst. Then, catalyst was added, and NH_3 (0.8 MPa) and H_2 (4 MPa) were introduced and reacted at 90 °C.

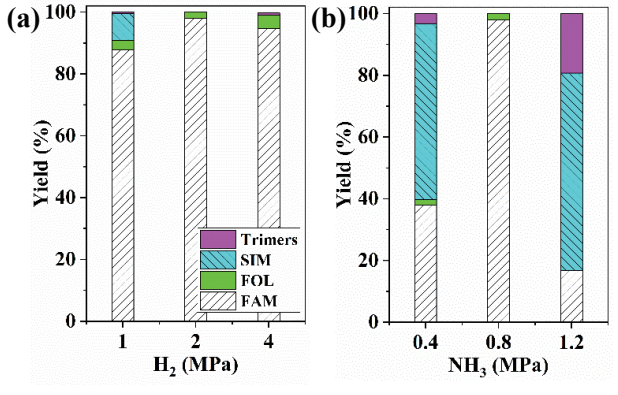

Figure 13 Influence of (a) H_2 and (b) NH_3 pressure. Reaction conditions: 5 mmol furfural, 5 mL *tert*-butanol, 0.1 g Ni/SiO_2-I-DP, 90 °C, and 1.5 h.

leading to the formation of trimer, and thus resulted in a decrease in the yield of FAM.

4 Conclusions

In conclusion, an efficient non-noble metal catalyst of Ni/SiO_2 catalyst was developed for reductive amination of furfural to furfurylamine, with it furfurylamine was produced with a high yield around 98%. The catalytic performance is closely relative to the structure and morphology of Ni nanoparticles and the acidity of the catalyst. Small Ni particle provides enough hydrogenation active sites, the Lewis acid sites and flat steps of Ni particles benefited to the adsorption and the hydrogenation of the intermediates of primary imine and *gem*-diamine to the final product of furfurylamine. On the surface of Ni/SiO_2-I-DP having higher acidity and smaller Ni particle with larger and more Ni flat step surface, the hydrogen was highly activated and the intermediates of PIM and *gem*-diamine were horizontal adsorbed to produce FAM selectively. As the reductive amination is complex containing several steps, if the Ni particle was too small, the hydrogenation activity was higher to produce more byproduct of FOL through FAL hydrogenation. While, if the activity was too low, more trimers could be formed and thus lowered the productivity. Thus, it is important to control the activity for obtaining high yield of the desired product in the reductive amination. These new findings provide helpful knowledge of the non-noble metal catalyst and the reductive animation reactions.

Acknowledgements

We gratefully acknowledge the financial support from the National Natural Science Foundation of China (Nos. 22172155 and 22072142) and the Youth Innovation Promotion Association CAS (No. 2016206).

Electronic Supplementary Material: Supplementary material (results comparison of reductive amination, STEM, TEM, XRD, H_2-TPD, NH_3-TPD, DRIFT spectra of CO adsorption, XPS, physical and chemical properties of catalysts, reusability of catalyst, and TGA) is available in the online version of this article at https://doi.org/10.1007/s12274-022-4923-0.

References

[1] Afanasyev, O. I.; Kuchuk, E.; Usanov, D. L.; Chusov, D. Reductive amination in the synthesis of pharmaceuticals. *Chem. Rev.* **2019**, *119*, 11857–11911.

[2] Froidevaux, V.; Negrell, C.; Caillol, S.; Pascault, J. P.; Boutevin, B. Biobased amines: From synthesis to polymers; present and future. *Chem. Rev.* **2016**, *116*, 14181–14224.

[3] Senthamarai, T.; Murugesan, K.; Schneidewind, J.; Kalevaru, N. V.; Baumann, W.; Neumann, H.; Kamer, P. C. J.; Beller, M.; Jagadeesh, R. V. Simple ruthenium-catalyzed reductive amination enables the synthesis of a broad range of primary amines. *Nat. Commun.* **2018**, *9*, 4123.

[4] Murugesan, K.; Wei, Z. H.; Chandrashekhar, V. G.; Neumann, H.; Spannenberg, A.; Jiao, H. J.; Beller, M.; Jagadeesh, R. V. Homogeneous cobalt-catalyzed reductive amination for synthesis of functionalized primary amines. *Nat. Commun.* **2019**, *10*, 5443.

[5] Li, H.; Guo, H. X.; Su, Y. Q.; Hiraga, Y.; Fang, Z.; Hensen, E. J. M.; Watanabe, M.; Smith, R. L. N-formyl-stabilizing quasi-catalytic species afford rapid and selective solvent-free amination of biomass-derived feedstocks. *Nat. Commun.* **2019**, *10*, 699.

[6] Irrgang, T.; Kempe, R. Transition-metal-catalyzed reductive amination employing hydrogen. *Chem. Rev.* **2020**, *120*, 9583–9674.

[7] Murugesan, K.; Senthamarai, T.; Chandrashekhar, V. G.; Natte, K.; Kamer, P. C. J.; Beller, M.; Jagadeesh, R. V. Catalytic reductive aminations using molecular hydrogen for synthesis of different kinds of amines. *Chem. Soc. Rev.* **2020**, *49*, 6273–6328.

[8] Saini, M. K.; Kumar, S.; Li, H.; Babu, S. A.; Saravanamurugan, S. Advances in the catalytic reductive amination of furfural to furfural amine: The momentous role of active metal sites. *ChemSusChem* **2022**, *15*, e202200107.

[9] Zou, H. T.; Chen, J. Z. Efficient and selective approach to biomass-based amine by reductive amination of furfural using Ru catalyst. *Appl. Catal. B: Environ.* **2022**, *309*, 121262.
[10] Das, K.; Shibuya, R.; Nakahara, Y.; Germain, N.; Ohshima, T.; Mashima, K. Platinum-catalyzed direct amination of allylic alcohols with aqueous ammonia: Selective synthesis of primary allylamines. *Angew. Chem., Int. Ed.* **2012**, *51*, 150–154.
[11] Liang, G. F.; Zhou, Y. G.; Zhao, J. P.; Khodakov, A. Y.; Ordomsky, V. V. Structure-sensitive and insensitive reactions in alcohol amination over nonsupported Ru nanoparticles. *ACS Catal.* **2018**, *8*, 11226–11234.
[12] Wang, B.; Ding, Y.; Lu, K.; Guan, Y. J.; Li, X. H.; Xu, H.; Wu, P. Host–guest chemistry immobilized nickel nanoparticles on zeolites as efficient catalysts for amination of 1-octanol. *J. Catal.* **2020**, *381*, 443–453.
[13] Fu, X. P.; Han, P. J.; Wang, Y. Z.; Wang, S.; Yan, N. Insight into the roles of ammonia during direct alcohol amination over supported Ru catalysts. *J. Catal.* **2021**, *399*, 121–131.
[14] Du, Y. D.; Chen, B. H.; Shu, W. Direct access to primary amines from alkenes by selective metal-free hydroamination. *Angew. Chem., Int. Ed.* **2021**, *60*, 9875–9880.
[15] Li, Y.; Shi, R. H.; Lin, W. W.; Cheng, H. Y.; Zhang, C.; Arai, M.; Zhao, F. Y. A green and recyclable ligand-free copper(I) catalysis system for amination of halonitrobenzenes in aqueous ammonia solution. *Mol. Catal.* **2019**, *475*, 110462.
[16] Feng, B. C.; Xi, B. H.; Zhang, Z. C.; Hou, Y. H.; Jin, Y.; Yao, Q. L. Production of heterocyclic primary amines from heterocyclic aldehydes on Ni-Mo/ZrO_2. *Chem. Eng. Technol.* **2022**, *45*, 1027–1035.
[17] Wu, J. J.; Darcel, C. Tandem Fe/Zn or Fe/In catalysis for the selective synthesis of primary and secondary amines via selective reduction of primary amides. *ChemCatChem* **2022**, *14*, e202101874.
[18] Lu, Q. Q.; Liu, J. G.; Ma, L. L. Recent advances in selective catalytic hydrogenation of nitriles to primary amines. *J. Catal.* **2021**, *404*, 475–492.
[19] Zhou, D.; Zhang, L. L.; Liu, X. Y.; Qi, H. F.; Liu, Q. G.; Yang, J.; Su, Y.; Ma, J. Y.; Yin, J. Z.; Wang, A. Q. Tuning the coordination environment of single-atom catalyst M-N-C towards selective hydrogenation of functionalized nitroarenes. *Nano Res.* **2022**, *15*, 519–527.
[20] Lu, G. P.; Sun, K. K.; Lin, Y. M.; Du, Q. X.; Zhang, J. W.; Wang, K.; Wang, P. C. Single-atomic-site iron on N-doped carbon for chemoselective reduction of nitroarenes. *Nano Res.* **2022**, *15*, 603–611.
[21] Lin, Y. M.; Nie, R. F.; Li, Y. T.; Wu, X.; Yu, J. Q.; Xie, S. H.; Shen, Y. J.; Mao, S. J.; Chen, Y. Z.; Lu, D. et al. Highly efficient and anti-poisoning single-atom cobalt catalyst for selective hydrogenation of nitroarenes. *Nano Res*., in press, https://doi.org/10.1007/s12274-022-4294-6.
[22] Feng, B. B.; Guo, R.; Cai, Q. L.; Song, Y. P.; Li, N.; Fu, Y. H.; Chen, D. L.; Zhang, J. W.; Zhu, W. D.; Zhang, F. M. Construction of isolated Ni sites on nitrogen-doped hollow carbon spheres with Ni-N_3 configuration for enhanced reduction of nitroarenes. *Nano Res.* **2022**, *15*, 6001–6009.
[23] Chang, P. J.; Cheng, H. Y.; Zhao, F. Y. Photocatalytic reduction of aromatic nitro compounds with Ag/Ag_xS composites under visible light irradiation. *J. Phys. Chem. C* **2021**, *125*, 26021–26030.
[24] Wu, Q. F.; Zhang, B.; Zhang, C.; Meng, X. C.; Su, X. L. N.; Jiang, S.; Shi, R. H.; Li, Y.; Lin, W. W.; Arai, M. et al. Significance of surface oxygen-containing groups and heteroatom P species in switching the selectivity of Pt/C catalyst in hydrogenation of 3-nitrostyrene. *J. Catal.* **2018**, *364*, 297–307.
[25] Gomez, S.; Peters, J. A.; Maschmeyer, T. The reductive amination of aldehydes and ketones and the hydrogenation of nitriles: Mechanistic aspects and selectivity control. *Adv. Synth. Catal.* **2002**, *344*, 1037–1057.
[26] Komanoya, T.; Kinemura, T.; Kita, Y.; Kamata, K.; Hara, M. Electronic effect of ruthenium nanoparticles on efficient reductive amination of carbonyl compounds. *J. Am. Chem. Soc.* **2017**, *139*, 11493–11499.
[27] Luo, D.; He, Y. R.; Yu, X.; Wang, F.; Zhao, J. J.; Zheng, W. T.; Jiao, H. J.; Yang, Y.; Li, Y. W.; Wen, X. D. Intrinsic mechanism of active metal dependent primary amine selectivity in the reductive amination of carbonyl compounds. *J. Catal.* **2021**, *395*, 293–301.
[28] Gould, N. S.; Landfield, H.; Dinkelacker, B.; Brady, C.; Yang, X.; Xu, B. J. Selectivity control in catalytic reductive amination of furfural to furfurylamine on supported catalysts. *ChemCatChem* **2020**, *12*, 2106–2115.
[29] Qi, H. F.; Liu, F.; Zhang, L. L.; Li, L.; Su, Y.; Yang, J. Y.; Hao, R.; Wang, A. Q.; Zhang, T. Modulating trans-imination and hydrogenation towards the highly selective production of primary diamines from dialdehydes. *Green Chem.* **2020**, *22*, 6897–6901.
[30] Gao, M. X.; Jia, X. Q.; Ma, J. P.; Fan, X. M.; Gao, J.; Xu, J. Self-regulated catalysis for the selective synthesis of primary amines from carbonyl compounds. *Green Chem.* **2021**, *23*, 7115–7121.
[31] Deng, D.; Kita, Y.; Kamata, K.; Hara, M. Low-temperature reductive amination of carbonyl compounds over Ru deposited on $Nb_2O_5 \cdot nH_2O$. *ACS Sustainable Chem. Eng.* **2019**, *7*, 4692–4698.
[32] Liang, G. F.; Wang, A. Q.; Li, L.; Xu, G.; Yan, N.; Zhang, T. Production of primary amines by reductive amination of biomass-derived aldehydes/ketones. *Angew. Chem., Int. Ed.* **2017**, *56*, 3050–3054.
[33] Dong, C. L.; Wang, H. T.; Du, H. C.; Peng, J. B.; Cai, Y.; Guo, S.; Zhang, J. L.; Samart, C.; Ding, M. Y. Ru/HZSM-5 as an efficient and recyclable catalyst for reductive amination of furfural to furfurylamine. *Mol. Catal.* **2020**, *482*, 110755.
[34] Guo, W. J.; Tong, T.; Liu, X. H.; Guo, Y.; Wang, Y. Q. Morphology-tuned activity of Ru/Nb_2O_5 catalysts for ketone reductive amination. *ChemCatChem* **2019**, *11*, 4130–4138.
[35] Chandra, D.; Inoue, Y.; Sasase, M.; Kitano, M.; Bhaumik, A.; Kamata, K.; Hosono, H.; Hara, M. A high performance catalyst of shape-specific ruthenium nanoparticles for production of primary amines by reductive amination of carbonyl compounds. *Chem. Sci.* **2018**, *9*, 5949–5956.
[36] Li, X. Y.; Le, S. D.; Nishimura, S. Reductive amination of 5-hydroxymethyl-2-furaldehyde over beta zeolite-supported ruthenium catalyst. *Catal. Lett.* **2021**, *152*, 2860–2868.
[37] Xie, C.; Song, J. L.; Hua, M. L.; Hu, Y.; Huang, X.; Wu, H. R.; Yang, G. Y.; Han, B. X. Ambient-temperature synthesis of primary amines via reductive amination of carbonyl compounds. *ACS Catal.* **2020**, *10*, 7763–7772.
[38] Qi, H. F.; Yang, J.; Liu, F.; Zhang, L. L.; Yang, J. Y.; Liu, X. Y.; Li, L.; Su, Y.; Liu, Y. F.; Hao, R. et al. Highly selective and robust single-atom catalyst Ru_1/NC for reductive amination of aldehydes/ketones. *Nat. Commun.* **2021**, *12*, 3295.
[39] Winans, C. F. Hydrogenation of aldehydes in the presence of ammonia. *J. Am. Chem. Soc.* **1939**, *61*, 3566–3567.
[40] Chen, W.; Sun, Y.; Du, J.; Si, Z. H.; Tang, X.; Zeng, X. H.; Lin, L.; Liu, S. J.; Lei, T. Z. Preparation of 5-(aminomethyl)-2-furanmethanol by direct reductive amination of 5-hydroxymethylfurfural with aqueous ammonia over the Ni/SBA-15 catalyst. *J. Chem. Technol. Biotechnol.* **2018**, *93*, 3028–3034.
[41] Hahn, G.; Kunnas, P.; de Jonge, N.; Kempe, R. General synthesis of primary amines via reductive amination employing a reusable nickel catalyst. *Nat. Catal.* **2019**, *2*, 71–77.
[42] Murugesan, K.; Beller, M.; Jagadeesh, R. V. Reusable nickel nanoparticles-catalyzed reductive amination for selective synthesis of primary amines. *Angew. Chem., Int. Ed.* **2019**, *58*, 5064–5068.
[43] Zhou, K.; Liu, H. Y.; Shu, H. M.; Xiao, S. W.; Guo, D. C.; Liu, Y. X.; Wei, Z. J.; Li, X. N. A comprehensive study on the reductive amination of 5-hydroxymethylfurfural into 2,5-bisaminomethylfuran over Raney Ni through DFT calculations. *ChemCatChem* **2019**, *11*, 2649–2656.
[44] Manzoli, M.; Gaudino, E. C.; Cravotto, G.; Tabasso, S.; Baig, R. B. N.; Colacino, E.; Varma, R. S. Microwave-assisted reductive amination with aqueous ammonia: Sustainable pathway using recyclable magnetic nickel-based nanocatalyst. *ACS Sustainable Chem. Eng.* **2019**, *7*, 5963–5974.
[45] Yuan, H. K.; Li, J. P.; Su, F. Z.; Yan, Z.; Kusema, B. T.; Streiff, S.; Huang, Y. J.; Pera-Titus, M.; Shi, F. Reductive amination of furanic aldehydes in aqueous solution over versatile Ni_yAlO_x catalysts. *ACS Omega* **2019**, *4*, 2510–2516.
[46] Zhang, Y. M.; Yang, H. M.; Chi, Q.; Zhang, Z. H. Nitrogen-doped

carbon-supported nickel nanoparticles: A robust catalyst to bridge the hydrogenation of nitriles and the reductive amination of carbonyl compounds for the synthesis of primary amines. *ChemSusChem* **2019**, *12*, 1246–1255.

[47] Zhou, K.; Chen, B. X.; Zhou, X. T.; Kang, S. M.; Xu, Y. J.; Wei, J. J. Selective synthesis of furfurylamine by reductive amination of furfural over Raney cobalt. *ChemCatChem* **2019**, *11*, 5562–5569.

[48] Liu, J. G.; Zhu, Y. T.; Wang, C. G.; Singh, T.; Wang, N.; Liu, Q. Y.; Cui, Z. B.; Ma, L. L. Facile synthesis of controllable graphene-co-shelled reusable Ni/NiO nanoparticles and their application in the synthesis of amines under mild conditions. *Green Chem.* **2020**, *22*, 7387–7397.

[49] Li, X. M.; Tian, J. Y.; Liu, H. L.; Tang, C. K.; Xia, C. G.; Chen, J.; Huang, Z. W. Effective synthesis of 5-amino-1-pentanol by reductive amination of biomass-derived 2-hydroxytetrahydropyran over supported Ni catalysts. *Chin. J. Catal.* **2020**, *41*, 631–641.

[50] Gokhale, T. A.; Raut, A. B.; Bhanage, B. M. Comparative account of catalytic activity of Ru- and Ni-based nanocomposites towards reductive amination of biomass derived molecules. *Mol. Catal.* **2021**, *510*, 111667.

[51] Dong, C. L.; Wu, Y. S.; Wang, H. T.; Peng, J. B.; Li, Y. Z.; Samart, C.; Ding, M. Y. Facile and efficient synthesis of primary amines via reductive amination over a Ni/Al_2O_3 catalyst. *ACS Sustainable Chem. Eng.* **2021**, *9*, 7318–7327.

[52] Klarner, M.; Blach, P.; Wittkämper, H.; de Jonge, N.; Papp, C.; Kempe, R. Key parameters for the synthesis of active and selective nanostructured 3d metal catalysts starting from coordination compounds-case study: Nickel mediated reductive amination. *ChemCatChem* **2021**, *13*, 3257–3261.

[53] Pan, Z. Y.; Zhang, Q.; Wang, W. Q.; Wang, L. L.; Wang, G. H. Size-tunable carbon-doped Ni nanoparticles for switchable reductive amination of biomass-derived carbonyl compounds to primary amines and secondary imines. *ACS Sustainable Chem. Eng.* **2022**, *10*, 3777–3786.

[54] Bhunia, M. K.; Chandra, D.; Abe, H.; Niwa, Y.; Hara, M. Synergistic effects of earth-abundant metal-metal oxide enable reductive amination of carbonyls at 50 °C. *ACS Appl. Mater. Interfaces* **2022**, *14*, 4144–4154.

[55] Zhuang, X. Z.; Liu, J. G.; Zhong, S. R.; Ma, L. L. Selective catalysis for the reductive amination of furfural toward furfurylamine by graphene-co-shelled cobalt nanoparticles. *Green Chem.* **2022**, *24*, 271–284.

[56] Jagadeesh, R. V.; Murugesan, K.; Alshammari, A. S.; Neumann, H.; Pohl, M. M.; Radnik, J.; Beller, M. MOF-derived cobalt nanoparticles catalyze a general synthesis of amines. *Science* **2017**, *358*, 326–332.

[57] Murugesan, K.; Chandrashekhar, V. G.; Senthamarai, T.; Jagadeesh, R. V.; Beller, M. Reductive amination using cobalt-based nanoparticles for synthesis of amines. *Nat. Protoc.* **2020**, *15*, 1313–1337.

[58] Yuan, Z. L.; Liu, B.; Zhou, P.; Zhang, Z. H.; Chi, Q. Preparation of nitrogen-doped carbon supported cobalt catalysts and its application in the reductive amination. *J. Catal.* **2019**, *370*, 347–356.

[59] Liu, J. M.; Guo, W. W.; Sun, H.; Li, R. Y.; Feng, Z. P.; Zhou, X. Y.; Huang, J. Reductive amination of carbonyl compounds with ammonia and hydrogenation of nitriles to primary amines with heterogeneous cobalt catalysts. *Chem. Res. Chin. Univ.* **2019**, *35*, 457–462.

[60] Liu, X. X.; Wang, Y. X.; Jin, S. W.; Li, X.; Zhang, Z. H. High performance of nitrogen-doped carbon-supported cobalt catalyst for the mild and selective synthesis of primary amines. *Arab. J. Chem.* **2020**, *13*, 4916–4925.

[61] Senthamarai, T.; Chandrashekhar, V. G.; Gawande, M. B.; Kalevaru, N. V.; Zbořil, R.; Kamer, P. C. J.; Jagadeesh, R. V.; Beller, M. Ultra-small cobalt nanoparticles from molecularly-defined Co-salen complexes for catalytic synthesis of amines. *Chem. Sci.* **2020**, *11*, 2973–2981.

[62] Sheng, M.; Fujita, S.; Yamaguchi, S.; Yamasaki, J.; Nakajima, K.; Yamazoe, S.; Mizugaki, T.; Mitsudome, T. Single-crystal cobalt phosphide nanorods as a high-performance catalyst for reductive amination of carbonyl compounds. *JACS Au* **2021**, *1*, 501–507.

[63] Elfinger, M.; Schönauer, T.; Thomä, S. L. J.; Stäglich, R.; Drechsler, M.; Zobel, M.; Senker, J.; Kempe, R. Co-catalyzed synthesis of primary amines via reductive amination employing hydrogen under very mild conditions. *ChemSusChem* **2021**, *14*, 2360–2366.

[64] Chandrashekhar, V. G.; Natte, K.; Alenad, A. M.; Alshammari, A. S.; Kreyenschulte, C.; Jagadeesh, R. V. Reductive amination, hydrogenation and hydrodeoxygenation of 5-hydroxymethylfurfural using silica-supported cobalt-nanoparticles. *ChemCatChem* **2022**, *14*, e202101234.

[65] Chen, X.; Jin, J. H.; Sha, G. Y.; Li, C.; Zhang, B. S.; Su, D. S.; Williams, C. T.; Liang, C. H. Silicon-nickel intermetallic compounds supported on silica as a highly efficient catalyst for CO methanation. *Catal. Sci. Technol.* **2014**, *4*, 53–61.

[66] Poncelet, G.; Centeno, M. A.; Molina, R. Characterization of reduced α-alumina-supported nickel catalysts by spectroscopic and chemisorption measurements. *Appl. Catal. A Gen.* **2005**, *288*, 232–242.

[67] Marceau, E.; Löfberg, A.; Giraudon, J. M.; Négrier, F.; Che, M.; Leclercq, L. From Al_2O_3-supported Ni(II)-ethylenediamine complexes to CO hydrogenation catalysts: Characterization of the surface sites and catalytic properties. *Appl. Catal. A Gen.* **2009**, *362*, 34–39.

[68] Mette, K.; Küehl, S.; Tarasov, A.; Willinger, M. G.; Kröhnert, J.; Wrabetz, S.; Trunschke, A.; Scherzer, M.; Girgsdies, F.; Düdder, H. et al. High-temperature stable Ni nanoparticles for the dry reforming of methane. *ACS Catal.* **2016**, *6*, 7238–7248.

[69] Agnelli, M.; Swaan, H. M.; Marquez-Alvarez, C.; Martin, G. A.; Mirodatos, C. CO hydrogenation on a nickel catalyst-II. A mechanistic study by transient kinetics and infrared spectroscopy. *J. Catal.* **1998**, *175*, 117–128.

[70] Hongmanorom, P.; Ashok, J.; Zhang, G. H.; Bian, Z. F.; Wai, M. H.; Zeng, Y. Q.; Xi, S. B.; Borgna, A.; Kawi, S. Enhanced performance and selectivity of CO_2 methanation over phyllosilicate structure derived Ni-Mg/SBA-15 catalysts. *Appl. Catal. B: Environ.* **2021**, *282*, 119564.

[71] Niu, J. T.; Wang, Y. L.; Liland, S. E.; Regli, S. K.; Yang, J.; Rout, K. R.; Luo, J.; Rønning, M.; Ran, J. Y.; Chen, D. Unraveling enhanced activity, selectivity, and coke resistance of Pt-Ni bimetallic clusters in dry reforming. *ACS Catal.* **2021**, *11*, 2398–2411.

[72] Arpini, B. H.; Braga, A. H.; Borges, L. R.; Vidinha, P.; Gonçalves, R. V.; Szanyi, J.; Rossi, L. M. Tuning CO_2 hydrogenation selectivity by N-doped carbon coating over nickel nanoparticles supported on SiO_2. *ACS Sustainable Chem. Eng.* **2022**, *10*, 2331–2342.

[73] Fischer, A.; Maciejewski, M.; Bürgi, T.; Mallat, T.; Baiker, A. Cobalt-catalyzed amination of 1,3-propanediol: Effects of catalyst promotion and use of supercritical ammonia as solvent and reactant. *J. Catal.* **1999**, *183*, 373–383.

[74] Krupka, J.; Dluhoš, L.; Mrózek, L. Evaluation of benzylamine production via reductive amination of benzaldehyde in a slurry reactor. *Chem. Eng. Technol.* **2017**, *40*, 870–877.